MULTISCALE AND MULTIORIENTATION FEATURE EXTRACTION WITH DEGENERATIVE PATTERNS FOR 3D NEUROIMAGING RETRIEVAL

Sidong Liu[1], *Weidong Cai*[1], *Lingfeng Wen*[1,2], *David Dagan Feng*[1,3]

[1] Biomedical and Multimedia Information Technology (BMIT) Research Group, School of Information Technologies, University of Sydney, Australia
[2] Department of PET and Nuclear Medicine, Royal Prince Alfred Hospital, Sydney, Australia
[3] Med-X Research Institute, Shanghai Jiao Tong University, China

ABSTRACT

Accurate neuroimaging feature extraction is essential for effective content-based management of the large neuroimaging databases, as well as achieving improved diagnosis. In this paper, we presented a multiscale and multi-orientation neuroimaging feature extraction algorithm with degenerative patterns for content-based 3D neuroimaging analysis and retrieval, based on the localized 3D Gabor wavelets. Our proposed approach was evaluated with 209 3D clinical neurological imaging studies and compared with the 3D discrete curvelet transform based method and the 3D spatial grey level co-occurrence matrices based method. The preliminary results suggested that our algorithm could support more reliable 3D neuroimaging retrieval.

Index Terms— feature extraction, neuroimaging retrieval, localized 3D Gabor wavelets

1. INTRODUCTION

Neuroimaging is a fundamental component of the neurological and neurosurgical diagnosis. It also has an important role in assessment of therapy and monitoring disease progression. Instrumentation advances, especially the introduction of the hybrid scanners, have resulted in markedly increased neuroimaging datasets and posed great challenges for image management and retrieval. Such challenges have prompted the research in the field of content-based image analysis and retrieval (CBIAR). CBIAR approaches supporting the visual, physiological features provide a solution complementary to traditional key-word based approaches [1].

A variety of feature extraction algorithms have been proposed to capture the intricate visual and physiological features in the neuroimaging data. These algorithms can be roughly classified into two categories, either based on spatial transforms or frequency transforms. Unay *et al.* [2] designed a brain structure-based region of interest (ROI) feature extraction approach using the local binary patterns (LBP) for brain magnetic resonance image (MRI) retrieval. Yu *et al.* [3] employed the spatial grey level co-occurrence matrices (GLCM) and neighborhood gray tone difference matrices (NGTDM) for head and neck tumor detection using PET (Positron Emission Tomography) - CT (Computed Tomography) imaging data. In our previous study, we proposed a volumetric feature extraction approach for PET retrieval based on the 3D-GLCM algorithm [4]. These spatial transform based methods rely heavily on the feature descriptors, e.g. for GLCM and NGTDM, there are first order features (mean, standard deviation, etc), second-order features (energy, entropy, etc), high-order features (coarseness, contrast, etc), and structure features (gradient mean, symmetrical ratio, etc) [3-5]. In addition, such spatial transforms are irreversible, thus the input images cannot be restored using the transform coefficients, which result in information loss.

The frequency transform based feature extraction approaches, on the other hand, analyze the data in frequency domain and the derived coefficients can be reversibly transformed back to spatial domain. Curvelet and Gabor filters are the two most widely used frequency transom based algorithms in computer vision. Curvelet is superior to wavelet and ridgelet in capturing higher dimensional singularities, ROI detection and image denoising [8-10]. In our recent study, we proposed two feature extraction approaches based on the 2D and 3D curvelet transforms [6, 7], respectively, and we found that the 3D discrete curvelet transform (3D-DCvT) was a promising tool in neuroimaging data analysis and retrieval. Both curvelets and Gabor wavelets decompose the frequency spectrum into sub-areas/volumes, but Gabor wavelets are further convolved with a Gaussian kernel function to optimally localize the impulse responses in both spatial and frequency domains, whereas curvelets do not have such property. Therefore, in this study, we proposed a neuroimaging feature extraction algorithm based on multiscale and multi-orientation Gabor wavelets. The effectiveness of our algorithm was validated by the localized retrieval of 209 3D neuroimaging studies with degenerative lesion patterns being extracted by t-maps, which comprise the voxel-by-voxel t-test statistics of these images. Two state-of-the-art algorithms, 3D-GLCM and 3D-DCvT, were also evaluated under the same condition.

2. METHODS

The framework of our proposed algorithm has four components, and the dataflow is demonstrated in Fig. 1.

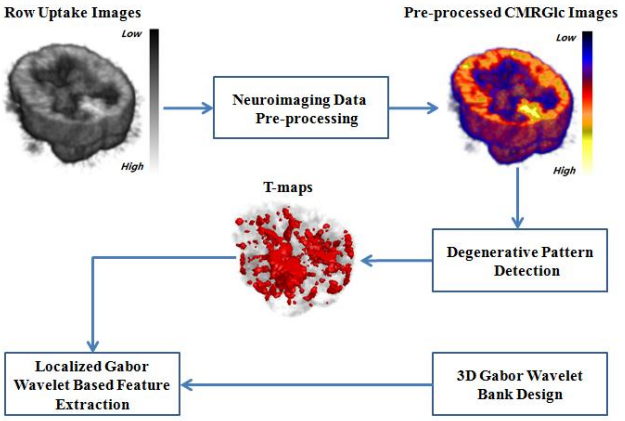

Fig. 1 The framework of our proposed feature extraction algorithm.

2.1. Neuroimaging data acquisition and pre-processing

The static FDG ([^{18}F]*2-fluoro-deoxy-glucose*) PET images were acquired on a CTI ECAT 951R whole body PET scanner. The autoradiographic (ARG) algorithm [12] was then employed to derive the Cerebral Metabolic Rate of Glucose (CMRGlc) parameters from these raw uptake images. Arterialized-venous blood samples were taken at 10 and 45 minutes post injection to calibrate a population-based input function. The generated CMRGlc images were spatial normalized to a standard space with dimensions of $91 \times 109 \times 91$ using SPM2 package (Wellcome Trust Centre for Neuroimaging, London, U.K.) [13]. To eliminate the gray tone variations between individual studies, we further divided the gray level values of the CMRGlc images by the mean value of the whole brain intensity, thus the imaging studies became directly comparable.

2.2. T-map based degenerative lesion detection

The degenerative lesion patterns are the key to characterize multiple types of neurological disorders. T-test was employed to compare the pre-processed CMRGlc images from each of the patient groups to those from the normal control group on a voxel-by-voxel basis, generating statistical parametric maps of group-related degernations in these CMRGlc images. In this study, 29 normal controls were used as t-test comparison samples and the significance level for t-test was set to 0.05, uncorrected for multiple comparisons. If the p-value of the voxel was less than the significance level, then the voxel was marked as a lesion voxel. Fig. 2 shows the lesion patterns of an Alzheimer's disease (AD) case, a vascular dementia (VD) case and a frontotemporal dementia (FTD) case, captured by t-maps. AD (first row) and VD (third row) showed a more extensive degenerative pattern than the FTD, and the pattern of AD also included the cerebellum and sub-cortical regions, whereas FTD (second row) mainly affected the frontal and temporal brain regions. The degenerative pattern differences between these sub-types of dementia were remarkable.

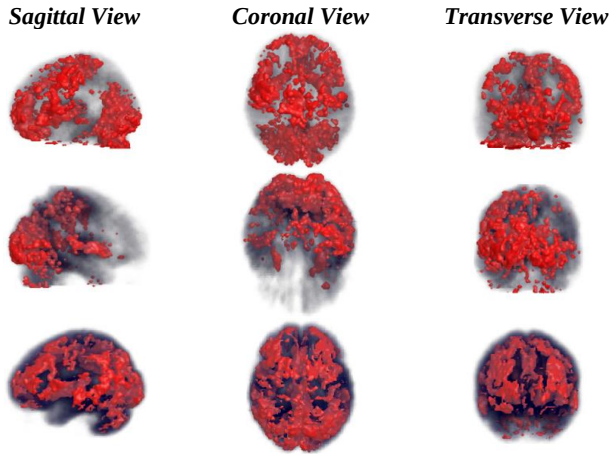

Fig. 2 The t-maps of an AD case (first row), a FTD case (second row) and a VD case (third row) in three different views.

2.3. 3D Gabor wavelet bank design

Gabor wavelets were proposed as a joint time-frequency analysis tool for one dimensional signal decomposition by Dennis Gabor [8]. Gabor wavelets offer the optimal simultaneous localization of both spatial and frequency information. Since Daugman *et al.* [11] discovered that analysis by Gabor functions was similar to perception in human visual system, the Gabor wavelets have been widely employed in various image processing applications. A 3D Gabor wavelet is an oriented complex sinusoidal wave modulated by a Gaussian function, as defined in (1) and (2):

$$g(x,y,z) = \tilde{g}(x,y,z) \times \exp\left[j2\pi(xu_0 + yv_0 + zw_0)\right] \quad (1)$$

$$\tilde{g}(x,y,z) = \Phi \times \exp\left[-\frac{(x^2+y^2+z^2)}{(2\sigma^2)}\right] \quad (2)$$

where $\Phi = -\frac{1}{(2\pi)^{3/2}\sigma^3}$ is the normalization factor, σ defines the width of the Gaussian, (u_0, v_0, w_0) is the center frequency with the peak magnitude, and j is the imaginary unit. The frequency response of such a Gabor wavelet is as defined in (3):

$$h(u,v,w) = \exp(-2\pi^2\sigma^2[(u-u_0)^2 + (v-v_0)^2 + (w-w_0)^2]) \quad (3)$$

The Gabor wavelet can also be defined in the spherical coordinate system as in (4):

$$g(*)_{f,\theta,\varphi} = \tilde{g}(*) \times \exp\left[j2\pi(xf\sin\theta\cos\varphi + yf\sin\theta\sin\varphi + zf\cos\theta\right) \quad (4)$$

where $f = \sqrt{u_0^2 + v_0^2 + w_0^2}$ is the radial center frequency, $u_0 = f\sin\theta\cos\varphi$, $v_0 = f\sin\theta\sin\varphi$, $w_0 = f\cos\theta$, $\theta = [0,\pi)$ is the orientation angle from w to the u-v plane, and $\varphi = [0,\pi)$ is the rotation angle around w axis. The Gabor wavelet with $\theta = 0$ and $\varphi = 0$ is always referred to as the mother wavelet.

Since the frequency and orientation of the images to be analyzed are usually unknown, a bank of Gabor wavelets are derived by rotating the mother Gabor wavelets to decompose the images at different scales and in different orientations. There are four parameters to define a Gabor wavelet bank, the number of decomposition scales (***S***), the number of orientations ($\boldsymbol{O_\theta}$ and $\boldsymbol{O_\varphi}$), and bandwidth in octave (***B***). Thus a Gabor wavelet bank, $G_{S,O_\theta,O_\varphi,B}$, shall cover a set of frequencies and orientations as in (5):

$$\{G_{S,O_\theta,O_\varphi,B} \coloneqq \mathrm{g}(*)_{f_t,\theta_p,\varphi_q}, t = 1,\dots,S;\ p = 1,\dots,O_\theta; q = 1,\dots,O_\varphi\} \quad (5)$$

where $f_t = \frac{f_{max}}{((2^{\mathrm{B}}+1)/(2^{\mathrm{B}}-1))^{t-1}}$, $\theta_p = \frac{(p-1)\pi}{O_\theta}$, and $\theta_q = \frac{(q-1)\pi}{O_\varphi}$. Theoretically, $G_{S,O_\theta,O_\varphi,B}$ should contain $S \times O_\theta \times O_\varphi$ wavelets, but there possibly exist some duplicated wavelets due to the advertent or inadvertent selection of the parameters. Fig. 3 (a) shows a Gabor wavelet bank with 5 scales, 8 orientations for both θ and φ, and bandwidth of 1 octave. There are 130 wavelets in total with no duplicates.

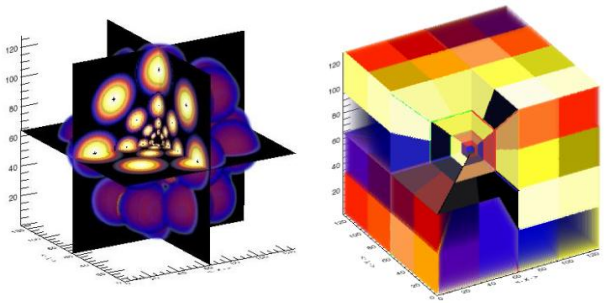

Fig. 3 (a) 3D-Gabor Bank (b) 3D-DCvT Bank
A Comparison of 3D -Gabor and -DCvT in frequency domain.

2.4. Localized Gabor wavelet based feature extraction

The t-maps were applied to all the CMRGlc images to extract the lesion region of interest. The 3D Gabor wavelets described in Section 2.3 were then used to generate the transform coefficients from these t-maps.

Convolution of 3D imaging data and the Gabor wavelets is very computationally expensive. According to the convolution theorem, convolution in one domain equals to the point-wise multiplication in the other domain. Therefore, we performed the multiplication of the 3D t-maps and the wavelet in frequency domain instead of the convolution in spatial domain. The image decomposition by 3D Gabor wavelets can be accomplished in three steps.

Step 1: for a given 3D t-map, $f(x,y,z), 0 \le x,y,z \le D$, where D is the image dimension, first apply the 3D fast Fourier transform (FFT) and obtain the Fourier samples, $f(u,v,w), -D/2 \le u,v,w \le D/2$.

Step 2: form the product $W(f,h) = f(u,v,w) \cdot h(u,v,w)$ for each f_t, θ_p, and φ_q.

Step 3: apply a 3D inverse FFT to each $W(f,h)$ hence generate a set of Gabor wavelet coefficients.

Totally 130 Gabor wavelets were used in this study, and the mean and standard deviation of the coefficients for each wavelet were computed to construct the feature vectors. Therefore, the representation of the localized Gabor wavelet based feature for each image is a 260-element vector.

3. EXPERIMENT AND RESULT

We evaluated our algorithm by using a dataset consisting of 209 (3D) neuroimaging studies acquired from a CTI ECAT 951R whole body PET scanner at the Department of PET and Nuclear Medicine, Royal Prince Alfred Hospital. Table 1 summarizes the composition of the dataset. AD, FTD and vascular dementia (VD) are the most commonly seen forms of dementia, and they accounted for over 50% of the total cases. Six other less common forms of dementia made up for another 25% of the dataset. Twelve indefinite AD/DLBD (suspicious AD or Diffuse Lewy Body Disease) cases were also included. We used the clinical diagnosis made by the experienced radiologists as the ground truth.

Table 1. The Dataset Summary.

Dementia	NO. of Cases (M:F)	Age($Mean \pm SD$)
AD	53 (20:33)	60.2±8.4
FTD	50 (29:21)	65.3±8.7
VD	10 (2:8)	50.9±14.4
AD/DLBD	15 (7:8)	65.7±8.5
Other	52(26:26)	67.8±10.2
Normal	29 (14:15)	54.9±15.8
Total	**209 (98:111)**	**63.5±9.2**

We conducted the retrieval of the top 3 most common forms of dementia, namely AD, FTD, and VD, using our proposed feature extraction algorithm. To verify the effectiveness of 3D Gabor wavelets, we compared our approach to the 3D- DCvT and 3D-GLCM algorithms under the same condition. 3D discrete curvelet bank was defined as having same scale and bandwidth parameters as the 3D Gabor wavelet bank. Fig. 3 (b) shows the frequency domain curvelet bank used in this study, and each wedge-shaped curvelet was painted with a unique color. The parameters for GLCM algorithm were set as three steps (1, 3, and 5 voxels) in 13 displacement directions, so totally 39 GLCMs were derived from one image. The Haralick feature descriptors [5] were used to quantize the GLCMs.

The similarity between any two images was calculated by the Euclidean distance on the normalized feature space [3]. We evaluated the performance using mean average precision (MAP), *i.e.*:

$$MAP = \sum_{n=1}^{N} p(n) \,/\mathrm{N} \quad (6)$$

where $p(n)$ is the average precision of each query and N is the total number of queries. The leave-one-out cross validation paradigm was used on AD, FTD and VD groups, so N was equal to the sum of cases in these three groups.

Fig. 4 shows the retrieval performance of three sub-types of dementia cases using the Gabor wavelets (blue), 3D-GLCM (red) and 3D-DCvT (green) algorithms. The last columns labeled 'Overall' suggest the average retrieval performance of all these three dementia groups, weighted by the number of cases in each group. The line segments (black) indicate the standard deviation for each method. It is clear that our proposed algorithm has the best performance and is as robust as the other two algorithms.

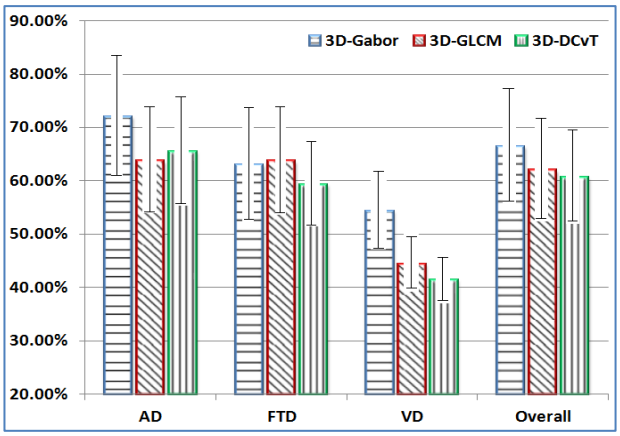

Fig. 4 The retrieval performance of three feature extraction algorithms.

The most striking improvement by using 3D Gabor wavelet is for the retrieval of VD cases (9.9% higher than 3D-GLCM and 12.9% higher than 3D-DCvT). The retrieval of AD cases is also very notable, since all three approaches achieve relatively high performances with the average precision above 63%, and the Gabor wavelets again have the best performance at 72.0%. For FTD cases, Gabor wavelets yield modest results slightly lower than 3D-GLCM algorithm by 0.7%, but still 3.8% higher than 3D-DCvT. Gabor wavelet benefits from Gaussian kernel function for joint localization in both spatial and frequency domains, therefore it can capture more sophisticated spatial and frequency variances than the other approaches.

4. CONCLUSION

In this paper, we present a multiscale and multi-orientation feature extraction approach with degenerative patterns for 3D neuroimaging data based on the localized 3D Gabor wavelet transforms. Our approach supports automatic brain degenerative lesion detection which is a key step to extract disease specific information. Compared with the other state-of-the-art 3D feature extraction methods, our algorithm achieved more reliable neuroimaging retrieval for most of the dementia sub-type cases, and has a great potential to be applied in many other applications, such as content analysis, image classification and computer aided diagnosis.

5. ACKNOLOEDGEMENT

This work was supported in part by ARC grants.

6. REFERENCES

[1] H. Muller, N. Michoux, D. Bandon and A. Geissbuhler, "A Review of Content-Based Image Retrieval Systems in Medical Applications – Clinical Benefits and Future Directions," *Int. J. of Med. Inf.*, vol. 73, pp.1-23, 2004.

[2] D. Unay, A. Ekin,and R. S. Jasinschi, "Local Structure-based Region of Interest Retrieval in Brain MR Images," *IEEE Trans. on Inf. Tech. in Biomed.*, vol. 14, issue. 4, pp.897-903, 2010.

[3] H. Yu, C. Caldwel, K. Mah and D. Mozeg, "Coregistered FDG PET/CT Base Textural Characterization of Head and Neck Cancer for Radiation Treatment Planning, " *IEEE Trans.* on *Med. Img.*, vol. 28, no. 3, pp. 374-383, Mar 2009.

[4] S. Liu, W. Cai, L. Wen, S. Eberl, M. Fulham and D. Feng, "A Robust Volumetric Feature Extraction Approach for 3D Neuroimaging Retrieval", *The 32nd Ann. Int. Conf. of the IEEE Eng. in Med. and Bio. Society*, pp. 5657-5660, 1-4 Sep 2010.

[5] R. M. Haralick, K. Shanmugam, I. Dinstein, "Texture features for image classification," *IEEE Trans. Sys., Man., and Cyb.*, vol. SMC-3, no. 6, 1973.

[6] S. Liu, L. Jing, W. Cai, L. Wen, S. Eberl, M. Fulham and D. Feng, "Localized Multiscale Texture Based Retrieval of Neurological Image", *The 23rd IEEE Int. Symposium on Comp-Based Med. Sys.*, pp. 243-248, Perth, Australia, 12-15 Oct 2010.

[7] S. Liu, W. Cai, L. Wen, S. Eberl, M. Fulham, and D. Feng, "Localized Functional Neuroimaging Retrieval using 3D Discrete Curvelet Transform", *IEEE Int. Symposium on Biomed. Img.*, pp. 1877-1880, Chicago, Illinois, USA, 30 March - 2 April 2011.

[8] E.J. Candes, D.L. Donoho, "Curvelets – A Surprisingly Effective Nonadaptive Representation for Objects with Edges", *Curves and Surfaces*, pp.105-120, Vanderbilt University Press, Nashville, TN, 2000.

[9] S. Alzubi, N. Islam and M. Abbod, "Multiresolution Analysis Using Wavelet, Ridgelet And Curvelet Transforms For Medical Imagingsegmentation," *Int. J. of Biomed. Img.*, 136034, Sep 2011.

[10] L. Dettori, L. Semler, "A comparison of wavelet, ridgelet and curvelet based texture classification algorithms in computed tomography", *Comp. in Bio. and Med.*, vol.37, pp.486- 498, 2007.

[11] John Daugman: "Complete Discrete 2-D Gabor Transforms by Neural Networks for Image Analysis and Compression", *IEEE Trans. on Acoustics, Speech, and Sig. Proc.* vol. 36. no. 7. pp. 1169-1179, July 1988.

[12] G.D. Hutchins, J.E. Holden, R.A. Koeppe, J.R. Halama, S.J. Gatley, and R.J. Nickles, "Alternative approach to single-scan estimation of cerebral glucose metabolic rate using glucose analogs with particular application to ischemia", *J. of Cere. Blood Flow and Meta.*, vol. 4, pp.35-40, 1984.

[13] R.S.J. Frackowiak, K.J. Friston, C.D. Frith, R.J. Dolan, C.J. Price, S. Zeki, J.T. Ashburner, and W.D. Penny, *Human Brain Function*. Amsterdam; Boston: Elsevier Academic Press, 2004.